

## Multiscale modeling of microwave-heated multiphase systems

Himanshu Goyal<sup>1</sup> and Dionisios G. Vlachos<sup>2\*</sup>

1. Department of Chemical Engineering, Indian Institute of Technology Madras, Chennai, Tamil Nadu 600036, India
2. Department of Chemical and Biomolecular Engineering, Catalysis Center for Energy Innovation, University of Delaware, 221 Academy Street, Newark, Delaware 19716, United States

### Abstract

Modeling of microwave heating of multiphase systems requires resolving the electromagnetic field from the single particle to the entire cavity. We introduce a multiscale methodology for computationally affordable simulations of microwave heating of multiphase systems consisting of one phase dispersed in a continuum phase. The methodology homogenizes the original multiphase system, by taking advantage of the large separation of length scales, to calculate the effective permittivity, effective thermal conductivity, and volumetric power absorbed in each phase. The methodology is rigorously assessed against particle-resolved detailed numerical simulations of model systems. We demonstrate a significant reduction in computational cost while retaining the accuracy of detailed simulations. The present methodology enables high throughput exploration of novel multiphase system designs utilizing microwave heating.

**Keywords:** microwave heating, multiscale modeling, numerical homogenization, multiphase reactors.

## 1. Introduction

Microwaves produced from renewable electricity provide a sustainable way of heating reactors, dryers, and other multiphase systems (hereafter called systems), thereby reducing the dependence on fossil fuels. Moreover, the rapid and selective heating of microwaves can intensify traditional processes leading to significant increase in productivity and energy efficiency, as shown in recent experimental studies [1-15].

Despite the abovementioned benefits, microwave heating is far from being widely implemented due to the poor understanding of the underlying processes, scalability, and cost issues. Many of the chemical processes utilize multiphase systems, such as a fixed bed or a slurry reactor, possessing multiple scales, ranging from an individual particle to the entire system. Experimental studies cannot easily provide the temperature profile across all scales [16]. Computations can be used to complement experiments and for the design, optimization, and scale-up of microwave reactors [17-19]. However, the complexity of microwave-heating of a multiphase system makes the modeling extremely challenging. For instance, non-spherical particles focus the electromagnetic field at their sharp edges and can result in hot spots and temperature gradients, implying that simulations need to resolve individual particles. The mere requirement of resolving all scales renders numerical simulations computationally prohibitive.

One way of overcoming the disparity in scales is the use of homogenization theory, a multiscale method applied chiefly in transport and specifically in diffusion [20-22] and thermal conduction [23, 24]. Homogenization theory takes advantage of the disparity in length scales and provides effective properties, thereby converting the original point-wise mathematical description into an averaged (coarse-grained) description. In the physics literature related to

metamaterials, calculating the effective electromagnetic properties, such as the electric permittivity, magnetic permeability, refractive index, and wave impedance, of structured composites is an active area of research [25-30]. For instance, analytical mixing formulae, such as the Clausius–Mossotti and the Maxwell–Garnett formulae [26], for computing effective properties for special cases and geometric simplifications, have been derived. Pendry et al. [25] derived the effective permeability of several simple periodic structures starting from the integral form of Maxwell’s equations. Liu et al. [28] evaluated the effective permittivity of a periodic composite structure by comparing the complex transmission coefficient with numerical calculations. However, the calculation of the effective permittivity based on the reflection and transmission coefficients is not unique [26]. When the inhomogeneity scale is small compared to the electromagnetic wavelength, the electrostatic limit has been used to calculate the effective permittivity, by comparing the energy stored in a capacitor containing the original multiphase system and the corresponding effective medium [27, 30]. Smith and Pendry [26] calculated the effective permittivity and permeability using a numerical homogenization scheme based on Pendry et al. [25].

The abovementioned techniques provide a way to evaluate the effective permittivity and permeability using homogenization theory and have mainly been explored by the metamaterials’ community. Microwave-heating of multiphase systems is a relatively new area of research and requires efficient simulation tools to evaluate the temperature distribution. At present, the finite element COMSOL multiphysics microwave simulation software is the most commonly used tool to investigate microwave heating [3, 17-19, 31, 32].

Here we develop the foundations of multiscale heat transfer for microwave heating of multiphase systems. Furthermore, we introduce a simple geometry for efficient particle-resolved simulations in COMSOL (hereafter called detailed simulations) and compare to the homogenization results of the coarse graining of ours as well as analytical formulae of prior work. We go beyond computing effective properties to look at the electric field, the power adsorbed, and the temperature distribution. The developed methodology allows for the first time computationally affordable numerical simulations of microwave heating of multiphase systems.

## 2. Coarse-graining Theory

We define the length scales of the multiphase system and the unit cell,  $\mathcal{L}_c$  and  $l_c$ , respectively, and consider the separation of length scales  $l_c \ll \mathcal{L}_c$ . Figure 1 shows the schematic of a multiphase system (e.g., a fixed bed or a slurry reactor) along with the associated length scales. The unit cell term is widely used in crystallography and materials science to represent the smallest periodic structure whose replication creates an entire material. Here the unit cell is defined as the length scale that captures statistically the inhomogeneity of the medium. The distribution of the material within the unit cell does not necessarily need to be periodic. The wavelength of the microwave  $\lambda$  is another important characteristic length scale. When the unit cell is much smaller than the characteristic length scales of the multiphase system, i.e.,  $\epsilon = l_c / \min(\lambda, \mathcal{L}_c) \ll 1$ , the governing equations can be transformed into averaged equations with effective coefficients [33]. This section describes the methodology to calculate the effective permittivity  $\epsilon_{\text{eff}}$ , effective thermal conductivity  $\kappa_{\text{eff}}$ , and volumetric power absorbed in the

dispersed  $\langle Q \rangle_d$  and continuous phases  $\langle Q \rangle_c$  of the effective medium obtained from the homogenization of the multiphase system.

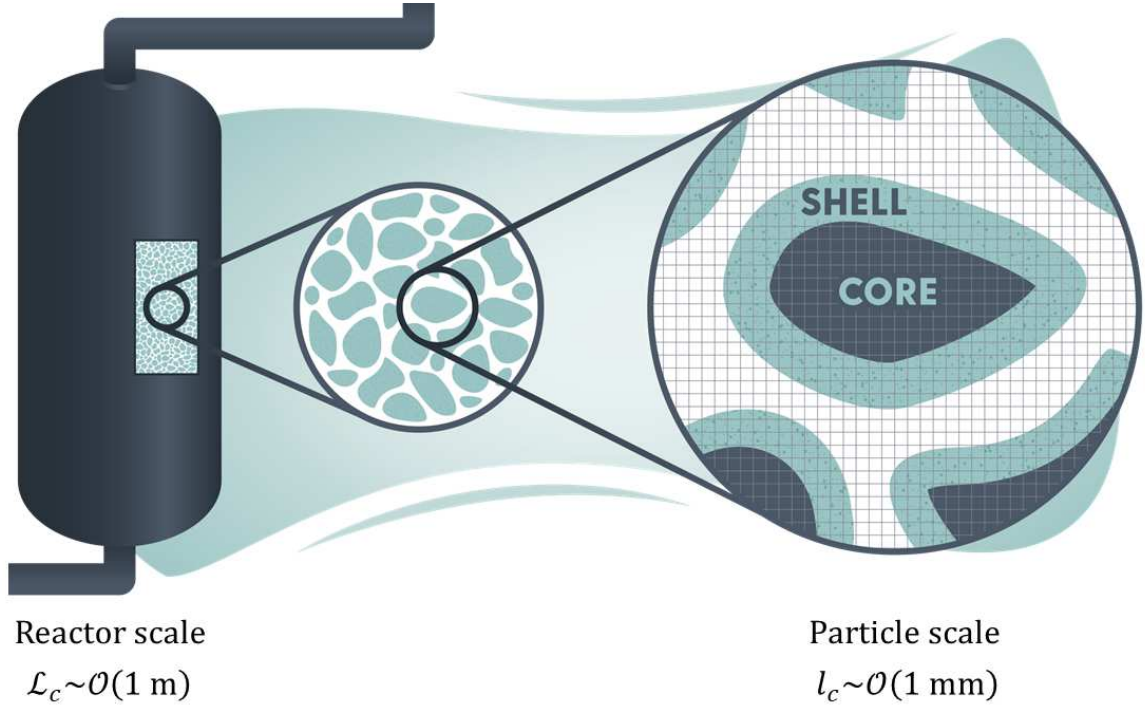


Figure 1: Schematic of the multiscale nature of a multiphase catalytic reactor. The largest length scale corresponds to the reactor-size  $\sim \mathcal{O}(1 \text{ m})$  and the smallest length scale is associated with a single particle  $\sim \mathcal{O}(1 \text{ mm})$ . Detailed simulations of a multiphase reactor require the mesh size to be sufficiently smaller than the particle size, thereby making the number of mesh elements too large to be computationally affordable.

## 2.1. Calculation of Effective Permittivity $\epsilon_{\text{eff}}$ via Homogenization Theory

Inside a source-free, linear, isotropic, and homogeneous medium, the Helmholtz equation describes the distribution of the electric and magnetic field components of a harmonic electromagnetic wave [34]

$$\begin{aligned} \nabla^2 \mathbf{E} + \omega^2 \mu \epsilon \mathbf{E} &= 0 \\ \nabla^2 \mathbf{H} + \omega^2 \mu \epsilon \mathbf{H} &= 0 \end{aligned} \quad (1)$$

where  $\mathbf{E}$  and  $\mathbf{H}$  are the electric and magnetic fields in phasor notation, respectively.  $\omega$  is the angular frequency and  $\varepsilon$  and  $\mu$  are the complex permittivity and permeability of the medium, respectively. The volumetric power absorbed  $Q$  [W/m<sup>3</sup>] due to dielectric heating is given by

$$Q = 0.5\omega\varepsilon''\mathbf{E}\cdot\mathbf{E}^* \quad (2)$$

where  $\varepsilon''$  is the imaginary part of the complex permittivity and  $\mathbf{E}^*$  is the complex conjugate of  $\mathbf{E}$ . The above equations need to be solved for each phase with appropriate interfacial conditions, requiring the mesh/grid to resolve the interface and thus making the computational cost of simulations extremely high. To reduce the computational cost, the governing equations are transformed into averaged equations by an averaging operation. For this purpose, the averaging operator  $\langle \cdot \rangle$  is defined over a length scale  $l_c$  as

$$\langle \cdot \rangle = \frac{1}{\mathcal{V}} \int_{\mathcal{V}} (\cdot) dV \quad (3)$$

Here,  $\mathcal{V}$  is the volume associated with the length scale  $l_c$ . The focus of this work is on dielectric heating; therefore, the magnetic permeability is assumed to be that of vacuum. Applying the averaging operator  $\langle \cdot \rangle$  on Eq. (1) for  $\mathbf{E}$  gives

$$\nabla^2 \langle \mathbf{E} \rangle + \omega^2 \mu \langle \varepsilon \mathbf{E} \rangle = 0 \quad (4)$$

Introducing an effective permittivity of the medium  $\varepsilon_{\text{eff}}$ , Eq. (4) becomes

$$\nabla^2 \langle \mathbf{E} \rangle + \omega^2 \mu \varepsilon_{\text{eff}} \langle \mathbf{E} \rangle = 0 \quad (5)$$

where

$$\varepsilon_{\text{eff}} = \frac{\langle \varepsilon \mathbf{E} \rangle}{\langle \mathbf{E} \rangle} \quad (6)$$

Eq. (5) governs the distribution of the averaged electric field  $\langle \mathbf{E} \rangle$ . Using the definition of the electric displacement field  $\mathbf{D}$

$$\mathbf{D} = \varepsilon \mathbf{E} \quad (7)$$

in Eq. (6) results in

$$\varepsilon_{\text{eff}} = \frac{\langle \mathbf{D} \rangle}{\langle \mathbf{E} \rangle} \quad (8)$$

Eq. (8) defines the effective permittivity  $\varepsilon_{\text{eff}}$  of a multiphase system. Using simulations, the local distribution of  $\mathbf{D}$  and  $\mathbf{E}$  is obtained within the unit cell and then used to calculate  $\varepsilon_{\text{eff}}$  according to Eq. (8).

## 2.2. Estimation of the Volumetric Power Absorbed [W/m<sup>3</sup>]

The point-wise volumetric power absorbed for the dispersed  $Q_d$  and continuum  $Q_c$  phases is given by

$$Q_d = 0.5\omega\varepsilon_d''(\mathbf{E} \cdot \mathbf{E}^*)_d \quad (9)$$

$$Q_c = 0.5\omega\varepsilon_c''(\mathbf{E} \cdot \mathbf{E}^*)_c$$

where  $\varepsilon_d''$  and  $\varepsilon_c''$  are the imaginary part of the permittivity of the dispersed and the continuum phases, respectively.  $(\mathbf{E} \cdot \mathbf{E}^*)_d$  and  $(\mathbf{E} \cdot \mathbf{E}^*)_c$  represent the strength of the electric field in the dispersed and continuum phases, respectively. Applying the averaging operator  $\langle \cdot \rangle$  to Eq. (9) provides

$$\langle Q \rangle_d = 0.5\omega\varepsilon_d''\langle \mathbf{E} \cdot \mathbf{E}^* \rangle_d \quad (10)$$

$$\langle Q \rangle_c = 0.5\omega\varepsilon_c''\langle \mathbf{E} \cdot \mathbf{E}^* \rangle_c$$

Since the simulations of the effective medium provide  $\langle \mathbf{E} \rangle$  instead of  $\mathbf{E}$ , we express  $\langle \mathbf{E} \cdot \mathbf{E}^* \rangle_d$  and  $\langle \mathbf{E} \cdot \mathbf{E}^* \rangle_c$  using  $\langle \mathbf{E} \rangle$ . For this purpose, the point-wise electric field  $\mathbf{E}$  is decomposed into the

averaged electric field  $\langle \mathbf{E} \rangle$  and the residual electric field  $\mathbf{E}'$ , reminiscent of theory for fluctuating and turbulent systems, such that

$$\mathbf{E} = \langle \mathbf{E} \rangle + \mathbf{E}' \quad (11)$$

Using Eq. (11),  $\langle \mathbf{E} \cdot \mathbf{E}^* \rangle$  can be expressed as

$$\langle \mathbf{E} \cdot \mathbf{E}^* \rangle = \langle \mathbf{E} \rangle \cdot \langle \mathbf{E}^* \rangle + \langle \mathbf{E}' \cdot \mathbf{E}'^* \rangle \quad (12)$$

By defining two numerically computed parameters  $\alpha$  and  $\beta$ :

$$\alpha = \frac{\langle \mathbf{E}' \cdot \mathbf{E}'^* \rangle}{\langle \mathbf{E} \rangle \cdot \langle \mathbf{E}^* \rangle} \quad (13)$$

$$\beta = \frac{\langle \mathbf{E} \cdot \mathbf{E}^* \rangle_d}{\langle \mathbf{E} \cdot \mathbf{E}^* \rangle}$$

$\langle \mathbf{E} \cdot \mathbf{E}^* \rangle_d$  and  $\langle \mathbf{E} \cdot \mathbf{E}^* \rangle_c$  can be calculated as

$$\langle \mathbf{E} \cdot \mathbf{E}^* \rangle_d = \beta(1 + \alpha) \langle \mathbf{E} \rangle \cdot \langle \mathbf{E}^* \rangle \quad (14)$$

$$\langle \mathbf{E} \cdot \mathbf{E}^* \rangle_c = \frac{(1 - \phi\beta)}{(1 - \phi)} (1 + \alpha) \langle \mathbf{E} \rangle \cdot \langle \mathbf{E}^* \rangle$$

where  $\phi$  is the volume fraction of the dispersed phase.  $\alpha$  and  $\beta$  capture the variation of  $\mathbf{E}$  at a length scale smaller than  $l_c$  and are calculated using the numerically evaluated  $\mathbf{E}$  within the unit cell. Substituting Eq. (14) into Eq. (10), we get

$$\langle Q \rangle_d = 0.5\omega\varepsilon_d''\beta(1 + \alpha) \langle \mathbf{E} \rangle \cdot \langle \mathbf{E}^* \rangle \quad (15)$$

$$\langle Q \rangle_c = 0.5\omega\varepsilon_c'' \frac{(1 - \phi\beta)}{(1 - \phi)} (1 + \alpha) \langle \mathbf{E} \rangle \cdot \langle \mathbf{E}^* \rangle$$

The total averaged volumetric power absorbed  $\langle Q \rangle_t$  is calculated by

$$\langle Q \rangle_t = \phi \langle Q \rangle_d + (1 - \phi) \langle Q \rangle_c \quad (16)$$

### 2.3. Estimation of the Effective Thermal Conductivity $\kappa_{\text{eff}}$ via Homogenization Theory

The temperature profile in a microwave field for convection-free systems is calculated by the energy conservation equation:

$$\rho C_p \frac{\partial T}{\partial t} + \nabla \cdot (\kappa \nabla T) = Q \quad (17)$$

where  $\rho$ ,  $C_p$ , and  $\kappa$  are the mass density, specific heat capacity, and thermal conductivity of the medium, respectively. The averaged energy conservation equation is given by [35]

$$(\rho C_p)_{\text{eff}} \frac{\partial T_{\text{avg}}}{\partial t} + \nabla \cdot (\kappa_{\text{eff}} \nabla T_{\text{avg}}) = \langle Q \rangle_t \quad (18)$$

Here  $(\rho C_p)_{\text{eff}}$  is equal to  $\langle \rho C_p \rangle$  as shown in Ref. [35] and  $\kappa_{\text{eff}}$  is calculated using the numerical homogenization technique described in Ref. [33]. The steady state heat conduction problem inside the unit cell is numerically solved in COMSOL and the resulting distribution of the temperature gradient is used to calculate  $\kappa_{\text{eff}}$  from the following expression [33]:

$$\kappa_{\text{eff}} = 8 \int_0^{1/2} \int_0^{1/2} \int_0^{1/2} \kappa(\xi_1, \xi_2, \xi_3) \frac{\partial T}{\partial \xi_1} d\xi_1 d\xi_2 d\xi_3 \quad (19)$$

Here,  $\kappa$  is a function of space.  $\xi_i$  are the *fast* variables defined as  $\xi_i = x_i/\epsilon$ ,  $x_i$  being the spatial coordinates with  $i = 1, 2, \text{ and } 3$ . A schematic of the multiscale methodology and details of the simulation setup to calculate  $\kappa_{\text{eff}}$  are provided in Sections S1 and S2 of the Supporting Information (SI), respectively. Equations (5) and (18) represent the homogenized description of microwave heating of a multiphase system. The temperature dependence of the dielectric properties and electromagnetic field dependence of the absorbed power make Eqs. (5) and (18) two-way coupled. It should be noted that without any loss of generality, the developed methodology can be used in more complex systems, where additional physics like fluid dynamics

is important, by integrating the appropriate governing equations with those of microwave heating.

### 3. Simulation Setup

Figure 2 shows the simulation setup, built in COMSOL, used to calculate the effective medium properties:  $\epsilon_{\text{eff}}$ ,  $\alpha$ , and  $\beta$ . A plane electromagnetic wave is generated from the inlet port propagating in the  $z$ -direction with the electric and magnetic fields fluctuating in the  $x$  and  $y$  directions, respectively. A perfectly matched layer (PML) boundary condition is employed at both ends of the domain in the  $z$ -direction that do not permit the reflection of microwaves. The  $x$  and  $y$  directions are made periodic. A number of unit cells are placed at the center of the domain.

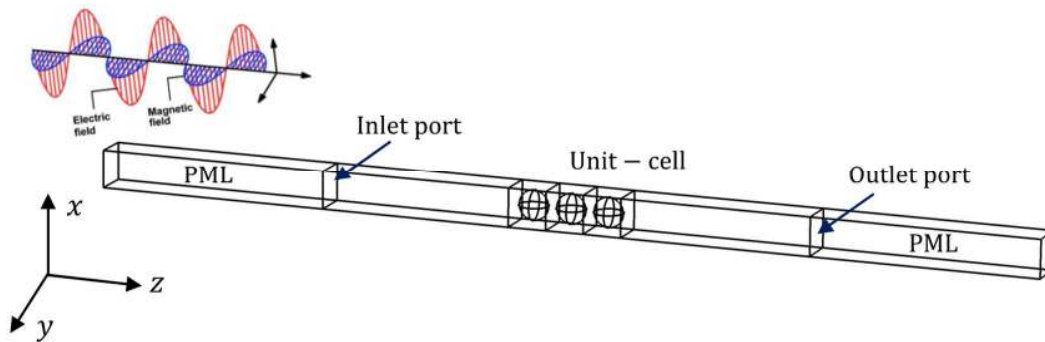


Figure 2. Computational setup to calculate the effective medium properties. Periodic boundary conditions are applied in the perpendicular  $x$ - $y$  directions. The incident wave propagates in the  $z$  direction.

A parametric study is performed to evaluate the effect of the PML thickness, the number of mesh elements, and the number of unit cells on  $\epsilon_{\text{eff}}$ . These results are provided in Section S3 of the SI. A domain of three unit cells with PML thickness of  $0.1\lambda$  and the gap between the port and PML boundary being equal to  $l_c$  is sufficient to evaluate the effective parameters.

For comparison of the coarse-grained (homogeneous phase) and detailed simulations, a computational setup consisting of twenty unit cells, shown in Figure 3, is used. In the detailed simulations, the multiphase system is fully resolved, i.e., the mesh size is sufficiently smaller than the dispersed particles, as shown in Figure 1. Even though our methodology is independent of the frequency of the microwaves, all the simulations performed here employ a frequency of 2.45 GHz, which is the most common frequency used for microwave heating.

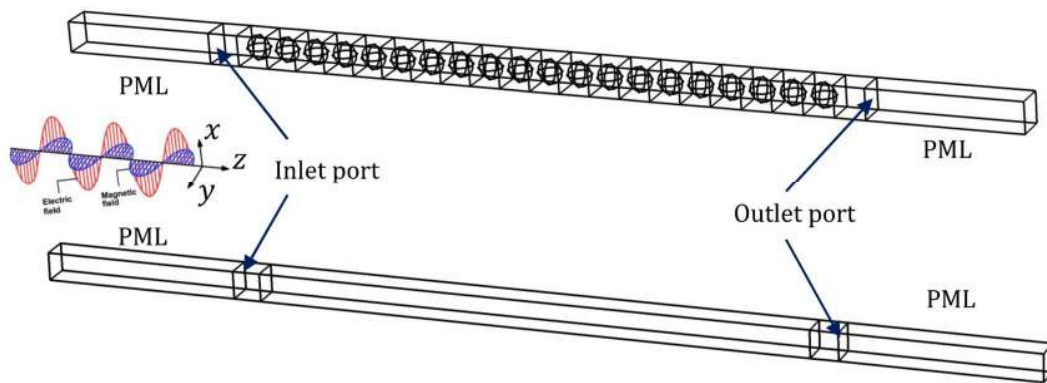


Figure 3: Computational setup for the coarse-grained and detailed simulations. Periodic boundary conditions are applied in the perpendicular  $x$ - $y$  directions. The incident wave propagates in the  $z$  direction. The domain is long enough to simulate a thin slab using computationally affordable calculations while capturing significant variation of the electromagnetic field.

#### 4. Assessment of the Multiscale Methodology

We compare the predicted effective permittivity  $\epsilon_{\text{eff}}$  against two established techniques from the literature as well as the electric field, the volumetric power absorbed, and the temperature profiles obtained from the coarse-grained and the detailed simulations.

Spherical particles uniformly dispersed in a continuum medium are chosen to represent the multiphase system. For verification, four combinations of dielectric properties of the dispersed and continuum phases are selected to cover a wide range of materials and achieve a sharp

contrast between the two phases. These values are provided in Table 1. For reference, at room temperature for a frequency of 2.45 GHz,  $\epsilon'$  and  $\tan\delta$  for water [17], a strong microwave absorber, are 78 and 0.13, respectively and for hexane [7], a weak microwave absorber, are 1.9 and 0.04, respectively. In case of solids,  $\epsilon'$  and  $\tan\delta$  for silicon carbide [31, 36] are 9.6 and 0.16, respectively and for Pyrex [32] are 3.3 and 0.01, respectively.

*Table 1. Dielectric constant and  $\tan\delta$  of the dispersed and continuum phases used in the simulations. Subscripts  $d$  and  $c$  refer to the dispersed and continuum phases, respectively.*

	Case 1	Case 2	Case3	Case 4
$\epsilon'_d$	100	100	2	2
$\tan\delta_d$	0.05	0.2	0.1	0.1
$\epsilon'_c$	2	2	100	100
$\tan\delta_c$	0.1	0.1	0.05	0.2

#### 4.1 Effective Permittivity Estimated via Various Methods

The effective permittivity  $\epsilon_{\text{eff}}$  calculated from our methodology is compared against the Maxwell-Garnett analytical mixing formula and the numerical homogenization technique of Myroshnychenko and Brosseau [30]. The Maxwell-Garnett formula is applicable to uniformly distributed spherical particles in the dilute limit  $\phi \rightarrow 0$ . The effective permittivity  $\epsilon_{\text{eff}}$  is calculated as

$$\epsilon_{\text{eff}} = \frac{2\phi(\epsilon_d - \epsilon_c) + \epsilon_d + 2\epsilon_c}{2\epsilon_c + \epsilon_d - \phi(\epsilon_d - \epsilon_c)} \quad (20)$$

where  $\epsilon_d$  and  $\epsilon_c$  are the permittivity of the dispersed and continuum phases, respectively. The numerical homogenization technique of Myroshnychenko and Brosseau [30] assumes a large

wavelength compared to the unit cell,  $l_c/\lambda \rightarrow 0$ , that is equivalent to the electrostatic limit, and estimates the effective permittivity based on the energy stored in the capacitor. Specifically, a parallel plate capacitor, with plates of area  $S$  and separation distance  $h$ , filled with a composite material is considered and a constant potential difference  $\varphi_0$  is maintained between the capacitor plates. The energy  $W$  stored in the capacitor is given by

$$W = \frac{1}{2} \int_{\Omega} \varepsilon [\nabla \varphi]^2 dA \quad (21)$$

where  $\Omega$  is the surface of the capacitor and  $\varphi$  is the local electrostatic potential. The energy stored  $W_{\text{eff}}$  in the capacitor containing a homogenous medium is given by:

$$W_{\text{eff}} = \frac{1}{2} \varepsilon_{\text{eff}} \frac{S}{h} \varphi_0^2 \quad (22)$$

By equating  $W$  and  $W_{\text{eff}}$ ,  $\varepsilon_{\text{eff}}$  is defined as

$$\varepsilon_{\text{eff}} = \frac{\int_{\Omega} \varepsilon [\nabla \varphi]^2 dA}{\frac{S}{h} \varphi_0^2} \quad (23)$$

The steady state electrostatic potential is numerically obtained in COMSOL to compute  $\varepsilon_{\text{eff}}$  using Eq. (23). Details of the simulation setup are provided in Section S4 of the SI.

The effective permittivity  $\varepsilon_{\text{eff}}$  is calculated using our methodology, the Maxwell-Garnett formula, and the methodology of Myroshnychenko and Brosseau [30] for the dielectric properties provided in Table 1. Figure 4 compares the real ( $\varepsilon'_{\text{eff}}$ ) and imaginary ( $\varepsilon''_{\text{eff}}$ ) components of the effective permittivity relative to the free space permittivity  $\varepsilon_0 = 8.85 \times 10^{-12}$  F/m as a function of the dispersed phase volume fraction  $\phi$ . The agreement among all the methods is excellent for low  $\phi$ . For higher  $\phi$ ,  $\varepsilon_{\text{eff}}$  obtained from our methodology and from that of Myroshnychenko and Brosseau [30] agree well but deviate from the Maxwell-Garnett formula.

This behavior is expected as the Maxwell-Garnett formula is valid in the limit  $\phi \rightarrow 0$ . Figure 4 shows that the value of  $\phi$  at which the Maxwell-Garnett formula fails depends strongly on the dielectric properties of the constituents. These results verify our methodology to predict  $\epsilon_{\text{eff}}$  against the established methods from the literature. Since the Maxwell-Garnett formula applies only to spherical particles, we evaluate the impact of particle shape on the effective permittivity in Section S5 of the SI. We find that particle shape has a significant impact on the effective permittivity, especially at higher particle volume fractions.

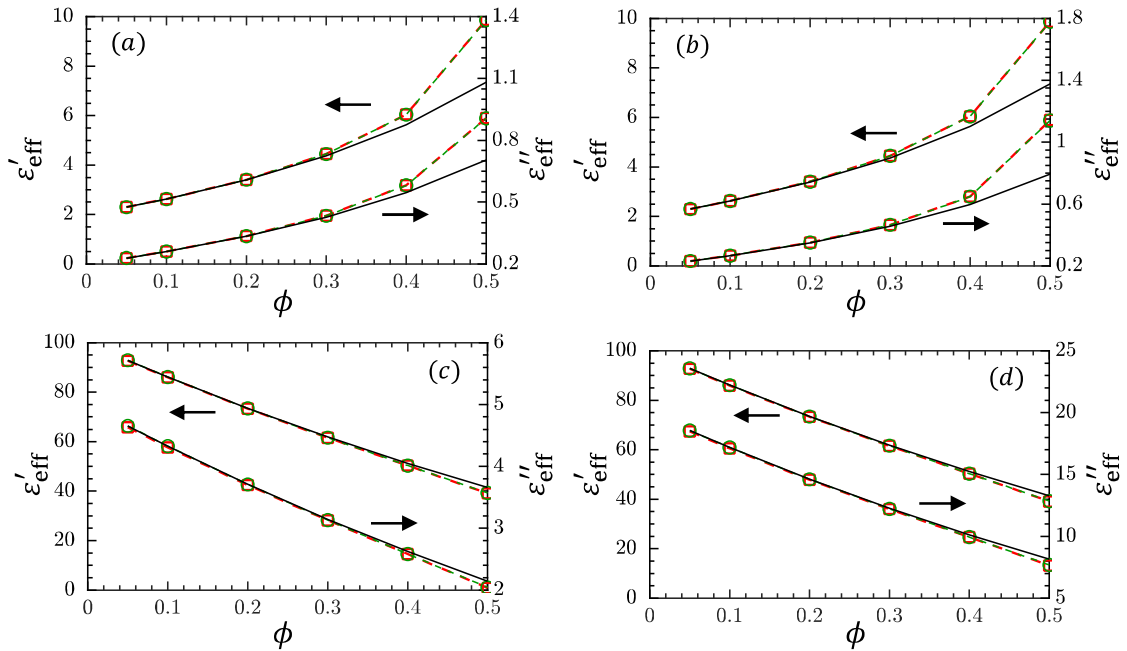


Figure 4. Real ( $\epsilon'_{\text{eff}}$ ) and imaginary ( $\epsilon''_{\text{eff}}$ ) components of the effective permittivity, relative to free space permittivity, obtained from our methodology (red squares with dashed lines), that of Myroshnychenko and Brosseau [30] (green circles with dashed lines), and the Maxwell-Garnett formula (solid black lines) as a function of the volume fraction of the dispersed phase  $\phi$  for spherical particles of diameter 1 mm. Properties of (a) Case 1, (b) Case 2, (c) Case 3, (d) Case 4 of Table 1.

## 4.2 Electric Field

Detailed simulations averaged using  $\langle \cdot \rangle$  (from Eq. (3)) are compared to coarse-grained (homogenization theory-based) simulations, using the simulation setup of Figure 3 with twenty

unit cells, corresponding to  $l_c/\mathcal{L}_c = 0.05$ . In the detailed simulations, volume fraction of the dispersed phase (spherical particles) is 0.25 and the input microwave power is 1 W. In Section S6 of the SI, we show that the differences between the coarse-grained and detailed simulations are below 10% when the maximum value of  $l_c/\lambda_c$  is lower than 0.1, where  $\lambda_c$  is the wavelength in the continuum medium. Four simulations are performed using cases 1 and 3 in Table 1 and two unit cell sizes, such that  $l_c/\lambda_c$  is 0.01 and 0.1. Figure 5 compares the real and imaginary parts of the electric field. The agreement is excellent. In Figure 5(c), where  $l_c/\lambda_c = 0.1$ , small differences are observed. Our results indicate that when the wavelength is larger than the unit cell by ten times or more, the proposed coarse-graining provides excellent results for the average electric field. For the commonly employed microwave frequency of 2.45 GHz,  $\lambda_c$  for water and air is 1.4 cm and 12.2 cm, respectively, implying that the maximum size of the unit cell should be  $\sim 1$  mm (in a high dielectric constant material) and  $\sim 1$  cm (in a low dielectric constant material). This size range encompasses a broad spectrum of multiphase systems in the chemical industry. For example, industrial fixed beds[37] contain pellets of size  $\mathcal{O}(1)$  mm, slurry reactors [38] use particle size of  $\mathcal{O}(1)$  mm, and fluidized beds [39] employ particles of size  $\mathcal{O}(0.1 - 1)$  mm.

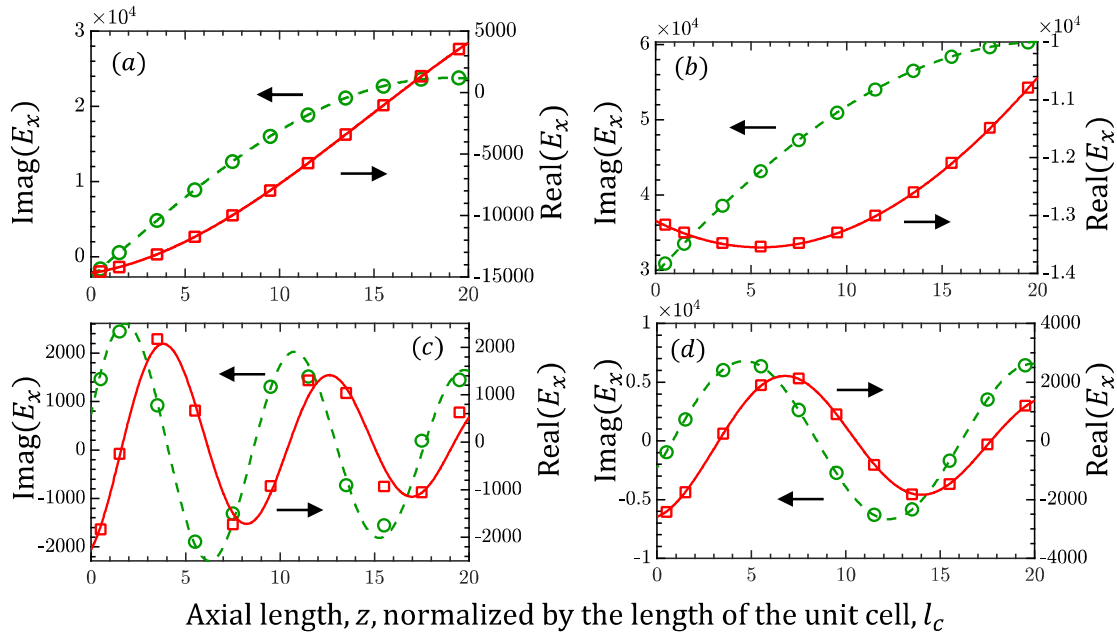


Figure 5. Real (red squares and solid lines) and imaginary (green circles and dashed lines) parts of the  $x$  component of the electric field obtained from the coarse-grained (lines) and detailed simulations (symbols) as a function of the normalized axial length. In the detailed simulations, spherical particles with  $\phi = 0.25$  and  $P_{in} = 1$  W are used. (a) Case 1 and  $l_c/\lambda_c=0.01$ , (b) Case 3 and  $l_c/\lambda_c=0.01$ , (c) Case 1 and  $l_c/\lambda_c=0.1$ , (d) Case 3 and  $l_c/\lambda_c=0.1$ . Cases 1 and 3 correspond to the dielectric properties provided in Table 1.

### 4.3 Volumetric Power Absorbed

Figure 6 compares the volumetric power absorbed by the dispersed  $\langle Q \rangle_d$  and the continuum  $\langle Q \rangle_c$  phases separately and combined  $\langle Q \rangle_t$ , obtained using the coarse-grained and detailed simulations with the simulation set-up and parameters of Section 4.2. Excellent agreement is found except for small differences when  $l_c/\lambda_c = 0.1$  (Figure 6(c)), emphasizing the need for  $l_c/\lambda_c \ll 1$  for accurate homogenization. In the detailed simulations, volume fraction of the dispersed phase (spherical particles) is 0.25 and the input microwave power is 1 W.

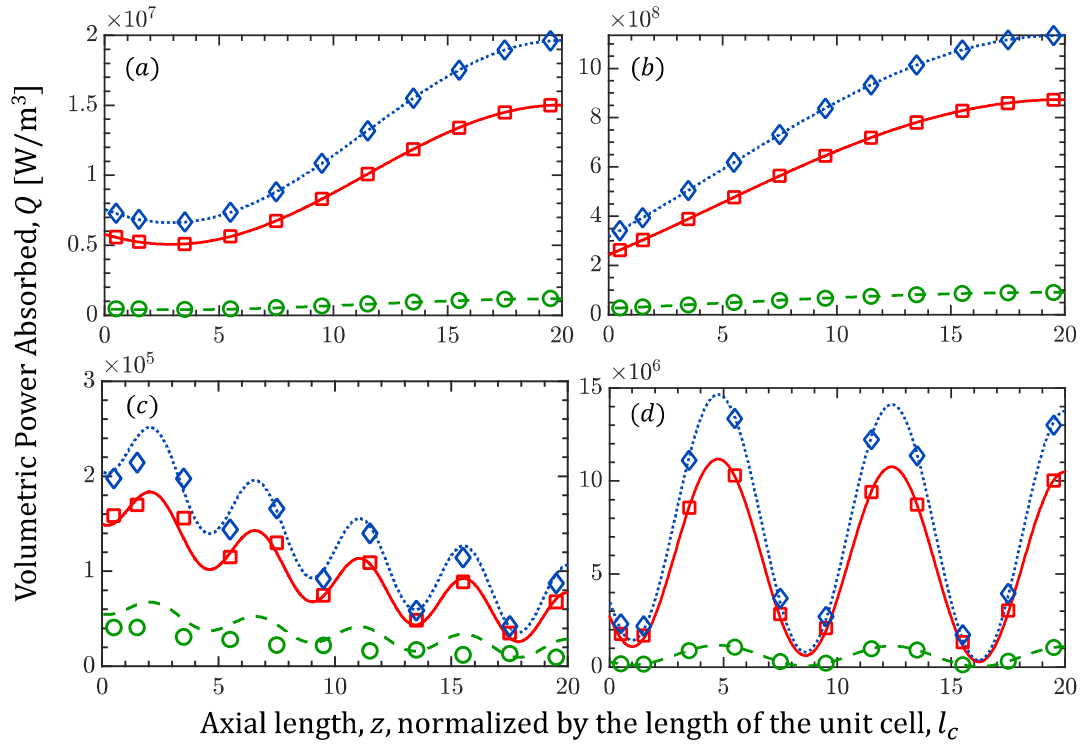


Figure 6. Averaged volumetric power absorbed by the dispersed phase  $\langle Q \rangle_d$  (green dashed lines and circles), the continuous phase  $\langle Q \rangle_c$  (blue dotted lines and diamonds), and both phases combined  $\langle Q \rangle_t$  (red solid lines and squares), as a function of the normalized axial length obtained from the coarse-grained (lines) and detailed (symbols) simulations. In the detailed simulations, spherical particles with  $\phi = 0.25$  and  $P_{in} = 1$  W are used. (a) Case 1 and  $l_c/\lambda_c=0.01$ , (b) Case 3 and  $l_c/\lambda_c=0.01$ , (c) Case 1 and  $l_c/\lambda_c=0.1$ , (d) Case 3 and  $l_c/\lambda_c=0.1$ . Cases 1 and 3 correspond to the dielectric properties provided in Table 1.

#### 4.4 Temperature Profiles

The ultimate goal is to predict the temperature profiles during microwave-heating. We compare the temperature profiles of coarse-grained and detailed simulations during transient microwave-heating using the simulation setup of Figure 3. Here, we assume that dielectric properties remain constant during the microwave-heating. In the detailed simulations, the density and specific heat capacity for both phases are  $10^3$  kg/m<sup>3</sup> and  $10^3$  J/Kg.K, respectively, representing the order of magnitude for a wide spectrum of liquids and solids. Spherical particles

of diameter  $500 \mu\text{m}$  represent the dispersed phase with a volume fraction of 0.25 and the input microwave power is 2 W. Three thermal conductivity values are used to cover a broad range of materials: 0.1 W/m.K (e.g., organic solvents, oils, Teflon, wood), 1 W/m.K (e.g., water, glass), and 10 W/m.K (e.g., alumina). In the coarse-grained simulations, the total volumetric power absorbed  $\langle Q \rangle_t$  and the effective thermal conductivity  $\kappa_{\text{eff}}$  are calculated using Eqs. (16) and (19), respectively, and employed in the spatially averaged energy conservation equation, Eq. (18). As an initial condition, the temperature of both phases is 293.15 K.

Figure 7 shows that the predicted temperature profiles of the two simulations after ten seconds of microwave-heating are in excellent agreement. As  $\kappa_{\text{eff}}$  increases, the temperature profile becomes more uniform across the domain. These results demonstrate the ability of coarse graining to accurately predict the coupled phenomena of electromagnetic field distribution, dielectric heat generation, and the temperature variation in space and time. It should be noted that in general, the dielectric properties change with temperature, requiring periodic evaluation of the effective permittivity during the simulations. In the transient simulations in COMSOL, the electromagnetic field is updated periodically when the change in permittivity is greater than a specified value. In a similar manner, the effective permittivity can be computed periodically before updating the electromagnetic field distribution.

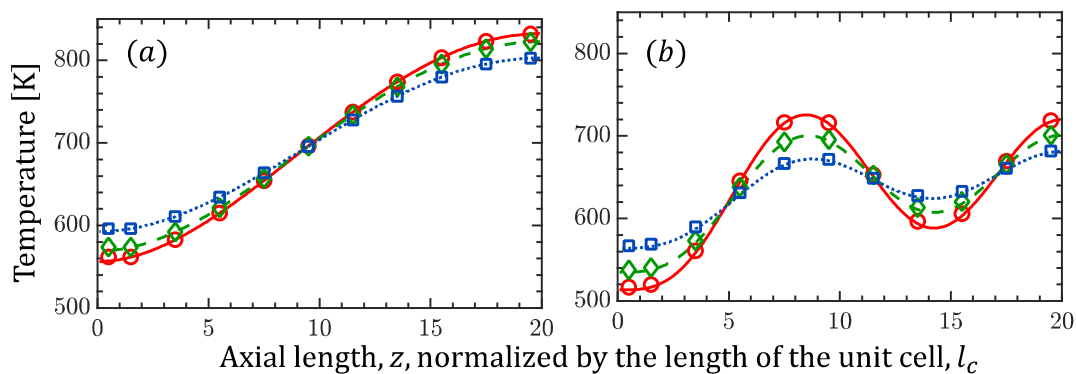


Figure 7. Temperature profiles from the coarse-grained (lines) and detailed (symbols) simulations along the normalized axial length. Three sets of thermal conductivity of the dispersed phase,  $\kappa_d$  and continuum phase,  $\kappa_c$  are used: 1)  $\kappa_d = 0.1, \kappa_c = 1, \kappa_{eff} = 0.71$  W/m.K (red circles and solid line), 2)  $\kappa_d = 1, \kappa_c = 1, \kappa_{eff} = 1$  W/m.K (green diamonds and dashed line), 3)  $\kappa_d = 10, \kappa_c = 1, \kappa_{eff} = 1.7$  W/m.K (blue squares and dotted line). In the detailed simulations, spherical particles of diameter  $500 \mu\text{m}$  are used with  $\phi = 0.25$  and  $P_{in} = 2$  W. Dielectric properties correspond to (a) Case 1 and (b) Case 3 of Table 1.

## 5. Reduction in the Computational Cost

In the detailed simulations, the need to resolve the dispersed phase puts a severe constraint on the mesh size leading to a large number of mesh elements. Our methodology allows a much coarser mesh size by homogenizing the multiphase system. Table 2 provides the computational cost of the transient microwave-heating simulations of Section 4.4. The simulations are performed on two cores of an iMac. The required number of mesh elements and compute time are reduced by more than a factor of 100 and 10, respectively, in comparison to the detailed simulations. This difference is expected to grow for much larger systems. The significant reduction in the computational memory and time requirement makes it possible to simulate microwave-heating of complex multiphase systems in a computationally affordable manner.

Table 2. Computational resources required to perform the transient microwave-heating simulations of Section 4.4.

	<i>Detailed simulation</i>	<i>Coarse-grained simulation</i>
<i>Number of mesh elements</i>	<i>42,000</i>	<i>250</i>
<i>Compute time (s)</i>	<i>135</i>	<i>10</i>

## 6. Toward Tuning and Optimization of the Effective Dielectric Properties of Multiphase Systems

Our methodology enables exploration of novel multiphase designs to achieve desirable microwave-heating. By tuning the structure (particle size, shape, and spatial arrangement), the effective dielectric properties can be optimized for desired performance. As a proof of concept, we consider two configurations consisting of cubic particles of size  $500 \mu\text{m}$ , shown in Figure 8(a), and evaluate their effective permittivity. In configuration 1, cubic particles are arranged uniformly with their faces parallel to each other, whereas in configuration 2, the edges of the cubic particles touch each other. The effective permittivity is calculated by varying the properties of the dispersed phase. This can be achieved for example by changing the fluid in the pores of the continuum solid, such as a monolith, or the type of solid immersed in a solvent. Figure 8(b) shows large deviation in the effective permittivity of the two configurations for a wide range of permittivity values of the dispersed phase.

The variation in the effective permittivity stems from the electric field distribution. Figure 8(c) shows the electric field intensity with dielectric properties corresponding to set 9 ( $\epsilon'_d=100$ ,  $\tan\delta_d=1$ ,  $\epsilon'_c=1$ ,  $\tan\delta_c=0$ ; see caption for all sets). The electric field varies significantly more in configuration 2. The localized concentration of the electric field is known to result in large deviations in the effective permittivity of the medium [25]. These results demonstrate the promise of the present methodology in exploiting quickly different configurations for microwave-heating. We propose that using an optimization algorithm, e.g., a genetic algorithm, one can vary the features of the unit cell in a multiphase system to optimize performance.

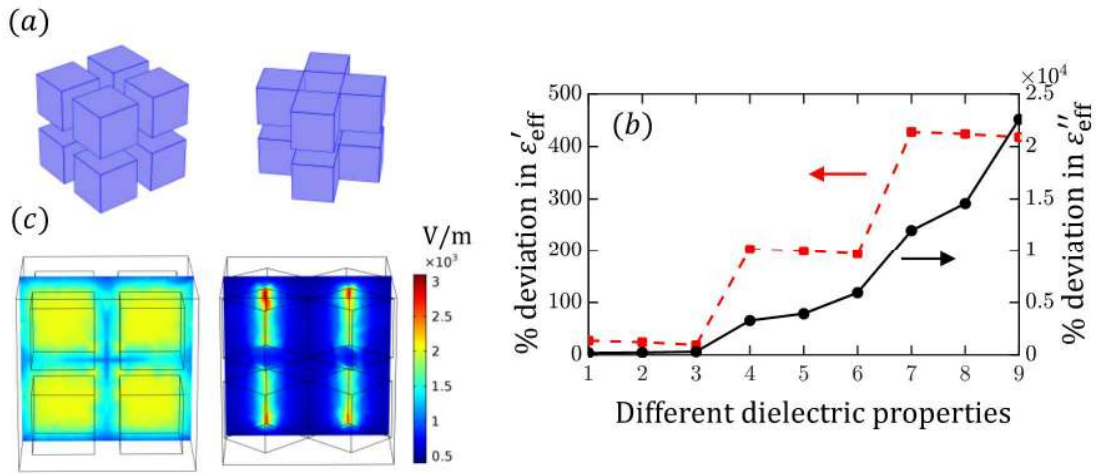


Figure 8: (a) Multiphase configurations 1 and 2 of identical particles arranged differently in space; (b) Percent deviation in the real and imaginary parts of the effective permittivity of configuration 2 from configuration 1. The relative permittivity of the continuum phase is equal to 1, whereas for the dispersed phase 9 sets of  $(\epsilon'_d, \tan\delta_d)$  are used in this order: (10,0.1) (10,0.5) (10,1) (50,0.1) (50,0.5) (50,1) (100,0.1) (100,0.5) (100,1). (c) Distribution of the electric field norm for configurations 1 and 2 for  $\epsilon'_d=100$  and  $\tan\delta_d=1$ .

## 7. Coarse-graining of Multiphase Systems without Resolving Temperature Gradients at the Microscale

In multiphase reactors, temperature gradients within the unit cell can significantly affect the reaction rate. Accurate predictions of reaction rates require resolving the temperature profile within the unit cell. Since the developed methodology cannot predict the sub-unit cell temperature field, we need to assess material properties and operating conditions for which the temperature is uniform within the unit cell. Under isothermal conditions at the unit cell scale, one does not need calculations to resolve the microscale, i.e., the coarse-grained simulations adequately resolve the temperature gradients at the reactor or process scale. For this purpose, we define two time scales, one associated with the rate of increase of the temperature difference

between any two points within the unit cell,  $\tau_{\text{inc}}$ , and one associated with the rate of thermal diffusion within the unit cell,  $\tau_{\text{diff}}$ .

We consider that the reaction rate within the unit cell varies significantly upon a 10 K variation in temperature (of course this depends on the activation energy of reactions); temperature non-uniformity between any two points of the unit cell matters when it is more than 10 K. The relevant time scales are defined as:

$$\begin{aligned}\tau_{\text{inc}} &\sim \frac{10 \text{ K}}{\Delta\dot{T}_{\text{max}}} \\ \tau_{\text{diff}} &\sim \frac{l_c^2}{\alpha}\end{aligned}\tag{24}$$

where  $\alpha$  is the thermal diffusivity, and  $\Delta\dot{T}_{\text{max}}$  is the maximum difference in the rate of temperature increase between two points within the unit cell. For the temperature non-uniformity within the unit cell to be negligible, we heuristically require that the thermal diffusion time scale to be short, i.e.,  $\tau_{\text{diff}} \ll \tau_{\text{inc}}$ , implying that

$$l_c \ll l_c^* = \sqrt{\frac{10\alpha}{\Delta\dot{T}_{\text{max}}}}\tag{25}$$

Based on the thermal diffusivity of the constituent materials and the observed heating rate, an upper limit on the unit cell size  $l_c^*$  can be calculated for the homogenization methodology to be accurate for reactive systems. In practice, we propose selecting  $l_c$  to be smaller than  $l_c^*$  by a factor of 2 or more.

We assess the time scale analysis by performing four detailed simulations of the microwave-heating of a spherical particle of diameter 1 mm placed in a continuum medium with  $\phi=0.25$  (parameters shown in Table 3). The dielectric properties of materials correspond to cases

1 and 3 of Table 1. The thermal diffusivity is chosen to be  $10^{-6}$  m<sup>2</sup>/s and  $10^{-4}$  m<sup>2</sup>/s, spanning materials ranging from gases to solids. In the majority of microwave-heating studies, the maximum rate of temperature increase  $\dot{T}_{\max}$  is  $\mathcal{O}(10^2)$  K/s [36, 40-44]. By assuming that  $\Delta\dot{T}_{\max}$  is  $\mathcal{O}(\dot{T}_{\max})$ ,  $\Delta\dot{T}_{\max} \sim \mathcal{O}(10^2)$  K/s. In the simulations, we select the input microwave power such that the average heating rate is about 100 K/s.

Table 3: Simulation parameters to calculate the intra-particle temperature profiles.

Parameter	Case 1	Case 2	Case 3	Case 4
Thermal diffusivity [m <sup>2</sup> /s]	$10^{-6}$	$10^{-6}$	$10^{-4}$	$10^{-4}$
$l_c^*$ [mm]	0.32	0.32	3.2	3.2
$l_c$ [mm]	1.3 ( $l_c > l_c^*$ )	1.3 ( $l_c > l_c^*$ )	1.3 ( $l_c < l_c^*$ )	1.3 ( $l_c < l_c^*$ )
$\epsilon'_d$	100	2	100	2
$\tan \delta_d$	0.05	0.1	0.05	0.1
$\epsilon'_c$	2	100	2	100
$\tan \delta_c$	0.1	0.05	0.1	0.05

Figure 9 shows the simulated intra-particle temperature profiles after five seconds of microwave-heating. As predicted by the time scale analysis, the temperature non-uniformity within the unit cell is significant ( $\sim 10$  K) for cases 1 and 2 where  $l_c > l_c^*$ , and negligible for cases 3 and 4 where  $l_c < l_c^*$ . These results are independent of the dielectric properties selected for the

constituent materials. Thus, Eq. (25) can be used to assess the applicability of our methodology to reactive multiphase systems at various experimental conditions.

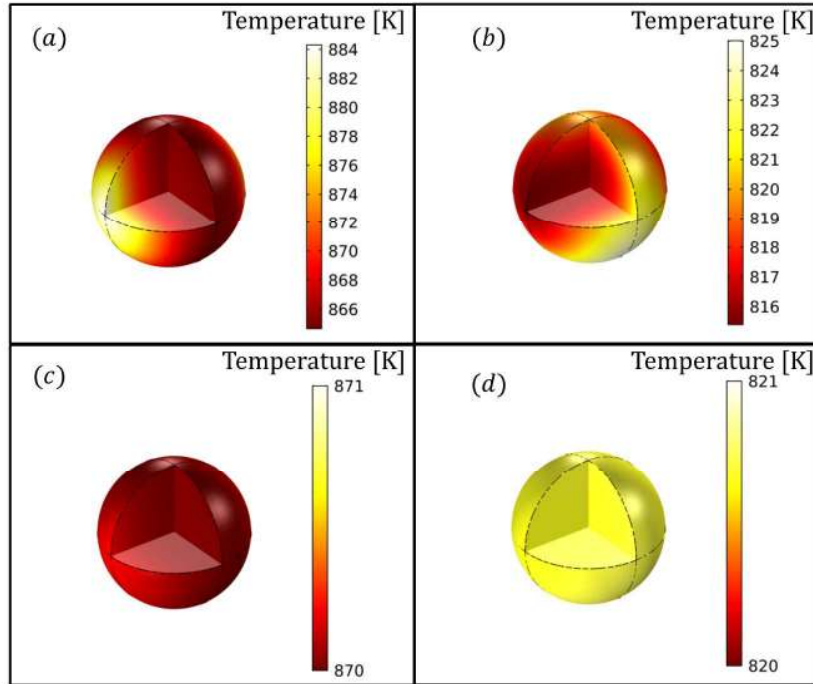


Figure 9: Intra-particle temperature profiles obtained from the detailed simulations of microwave-heating of spherical particles of diameter 1 mm with  $\phi=0.25$ . (a) Case 1 ( $l_c > l_c^*$ ), (b) Case 2 ( $l_c > l_c^*$ ), (c) Case 3 ( $l_c < l_c^*$ ), (d) Case 4 ( $l_c < l_c^*$ ) with properties from Table 3.

## 8. Conclusions

We introduced numerical homogenization as an effective multiscale methodology to numerically simulate microwave heating of complex multiphase systems in a computationally efficient manner. The original electromagnetic equations are transformed into spatially coarse-grained equations with effective parameters, and a unit cell is defined to compute the effective properties. The unit cell size should be sufficiently ‘large’ to statistically capture the inhomogeneity of the medium but small compared to the electromagnetic wavelength.

Comparison with the Maxwell–Garnett formula indicates that the latter is a good approximation for certain cases and unexpectedly up to relatively high densities of the dispersed phase. Thus, it can serve as a first approximation in design. Detailed simulations were used to verify our methodology and demonstrate the significant reduction achieved in the computational cost. The methodology can easily be implemented in COMSOL or any other multiphysics numerical solver.

Our methodology could also be applied to reactive multiphase systems when the unit cell size is smaller than a critical length, which depends on the thermal diffusivity and the heating rate of the material. The coarse-grained simulations need to be solved only at the process scale and accurately predict the distribution of the electric field, volumetric power absorbed, and temperature during transient microwave-heating. We discuss the potential of applying our methodology to modeling structured multiphase systems whose constituent materials have widely varying dielectric properties and ultimately to optimizing structures.

### **Supporting Information**

The Supporting Information is available free of charge on the Elsevier publications website.

### **Author Information**

Corresponding Author

\*Email: vlachos@udel.edu

### **Acknowledgements**

This work was supported by the RAPID manufacturing institute, supported by the Department of Energy (DOE), award number DE-EE0007888-8.3. The Delaware Energy Institute is grateful to the State of Delaware for its support of the RAPID institute projects.

## References

- [1] G. S. J. Sturm, M. D. Verweij, A. I. Stankiewicz, and G. D. Stefanidis, "Microwaves and microreactors: design challenges and remedies," *Chemical Engineering Journal*, vol. 243, pp. 147-158, 2014.
- [2] A. Ramirez, J. L. Hueso, M. Abian, M. U. Alzueta, R. Mallada, and J. Santamaria, "Escaping undesired gas-phase chemistry: Microwave-driven selectivity enhancement in heterogeneous catalytic reactors," *Science advances*, vol. 5, no. 3, p. eaau9000, 2019.
- [3] M. De Bruyn *et al.*, "Subtle microwave-induced overheating effects in an industrial demethylation reaction and their direct use in the development of an innovative microwave reactor," *Journal of the American Chemical Society*, vol. 139, no. 15, pp. 5431-5436, 2017.
- [4] I. Julian, H. Ramirez, J. L. Hueso, R. Mallada, and J. Santamaria, "Non-oxidative methane conversion in microwave-assisted structured reactors," *Chemical Engineering Journal*, vol. 377, p. 119764, 2019.
- [5] S. Horikoshi, M. Kamata, and N. Serpone, "Energy Savings through Microwave Selective Heating of Pd/AC Catalyst Particulates in a Fixed-Bed Reactor," *Chemical Engineering & Technology*, vol. 39, no. 8, pp. 1575-1577, 2016.
- [6] S. Horikoshi, M. Kamata, T. Sumi, and N. Serpone, "Selective heating of Pd/AC catalyst in heterogeneous systems for the microwave-assisted continuous hydrogen evolution from organic hydrides: Temperature distribution in the fixed-bed reactor," *International Journal of Hydrogen Energy*, vol. 41, no. 28, pp. 12029-12037, 2016.
- [7] C. O. Kappe, D. Dallinger, and S. S. Murphree, "Practical microwave synthesis for organic chemists," *Strategies, Instruments, and Protocols (Wiley-VCH, Weinheim, Germany, 2009)*, 2009.
- [8] F. Motasemi and M. T. Afzal, "A review on the microwave-assisted pyrolysis technique," *Renewable and Sustainable Energy Reviews*, vol. 28, pp. 317-330, 2013.
- [9] A. M. Parvez, T. Wu, M. T. Afzal, S. Mareta, T. He, and M. Zhai, "Conventional and microwave-assisted pyrolysis of gumwood: A comparison study using thermodynamic evaluation and hydrogen production," *Fuel processing technology*, vol. 184, pp. 1-11, 2019.
- [10] T. D. Musho, C. Wildfire, N. M. Houlihan, E. M. Sabolsky, and D. Shekhawat, "Study of Cu<sub>2</sub>O particle morphology on microwave field enhancement," *Materials Chemistry and Physics*, vol. 216, pp. 278-284, 2018.
- [11] H. Li *et al.*, "Breaking the equilibrium at the interface: microwave-assisted reactive distillation (MARD)," *Reaction Chemistry & Engineering*, vol. 4, no. 4, pp. 688-694, 2019.
- [12] H. Li, J. Liu, X. Li, and X. Gao, "Microwave-induced polar/nonpolar mixture separation performance in a film evaporation process," *AIChE Journal*, vol. 65, no. 2, pp. 745-754, 2019.
- [13] R. Cherbański and E. Molga, "Intensification of desorption processes by use of microwaves—an overview of possible applications and industrial perspectives," *Chemical Engineering and Processing: Process Intensification*, vol. 48, no. 1, pp. 48-58, 2009.

- [14] R. Cherbański, "Regeneration of granular activated carbon loaded with toluene—comparison of microwave and conductive heating at the same active powers," *Chemical Engineering and Processing-Process Intensification*, vol. 123, pp. 148-157, 2018.
- [15] R. Manno, V. Sebastian, R. Mallada, and J. s. Santamaria, "110th Anniversary: Nucleation of Ag Nanoparticles in Helical Microfluidic Reactor. Comparison between Microwave and Conventional Heating," *Industrial & Engineering Chemistry Research*, vol. 58, no. 28, pp. 12702-12711, 2019.
- [16] L. S. Gangurde, G. S. J. Sturm, T. J. Devadiga, A. I. Stankiewicz, and G. D. Stefanidis, "Complexity and challenges in noncontact high temperature measurements in microwave-assisted catalytic reactors," *Industrial & engineering chemistry research*, vol. 56, no. 45, pp. 13379-13391, 2017.
- [17] G. S. J. Sturm, M. D. Verweij, T. Van Gerven, A. I. Stankiewicz, and G. D. Stefanidis, "On the effect of resonant microwave fields on temperature distribution in time and space," *International Journal of Heat and Mass Transfer*, vol. 55, no. 13-14, pp. 3800-3811, 2012.
- [18] G. S. J. Sturm, M. D. Verweij, T. Van Gerven, A. I. Stankiewicz, and G. D. Stefanidis, "On the parametric sensitivity of heat generation by resonant microwave fields in process fluids," *International Journal of Heat and Mass Transfer*, vol. 57, no. 1, pp. 375-388, 2013.
- [19] H. Goyal, A. Mehdad, R. F. Lobo, G. D. Stefanidis, and D. G. Vlachos, "Scaleup of a Single-Mode Microwave Reactor," *Industrial & Engineering Chemistry Research*, 2019/10/21 2019, doi: 10.1021/acs.iecr.9b04491.
- [20] S. R. Deshmukh, A. B. Mhadeshwar, M. I. Lebedeva, and D. G. Vlachos, "From density functional theory to microchemical device homogenization: model prediction of hydrogen production for portable fuel cells," *International Journal for Multiscale Computational Engineering*, vol. 2, no. 2, 2004.
- [21] J. E. Rim, P. M. Pinsky, and W. W. van Osdol, "Using the method of homogenization to calculate the effective diffusivity of the stratum corneum," *Journal of Membrane Science*, vol. 293, no. 1-2, pp. 174-182, 2007.
- [22] J. L. Auriault and J. Lewandowska, "Homogenization analysis of diffusion and adsorption macrotransport in porous media: macrotransport in the absence of advection," *Geotechnique*, vol. 43, no. 3, pp. 457-469, 1993.
- [23] A. Dasgupta and R. K. Agarwal, "Orthotropic thermal conductivity of plain-weave fabric composites using a homogenization technique," *Journal of Composite Materials*, vol. 26, no. 18, pp. 2736-2758, 1992.
- [24] Y. Asakuma, S. Miyauchi, T. Yamamoto, H. Aoki, and T. Miura, "Homogenization method for effective thermal conductivity of metal hydride bed," *International Journal of Hydrogen Energy*, vol. 29, no. 2, pp. 209-216, 2004.
- [25] J. B. Pendry, A. J. Holden, D. J. Robbins, and W. J. Stewart, "Magnetism from conductors and enhanced nonlinear phenomena," *IEEE transactions on microwave theory and techniques*, vol. 47, no. 11, pp. 2075-2084, 1999.
- [26] D. R. Smith and J. B. Pendry, "Homogenization of metamaterials by field averaging," *JOSA B*, vol. 23, no. 3, pp. 391-403, 2006.
- [27] N. Jebbor and S. Bri, "Effective permittivity of periodic composite materials: Numerical modeling by the finite element method," *Journal of Electrostatics*, vol. 70, no. 4, pp. 393-399, 2012.

- [28] L. Liu, S. M. Matitsine, Y. B. Gan, and K. N. Rozanov, "Effective permittivity of planar composites with randomly or periodically distributed conducting fibers," *Journal of applied physics*, vol. 98, no. 6, p. 063512, 2005.
- [29] D. J. Bergman, "The dielectric constant of a composite material—a problem in classical physics," *Physics Reports*, vol. 43, no. 9, pp. 377-407, 1978.
- [30] V. Myroshnychenko and C. Brosseau, "Finite-element method for calculation of the effective permittivity of random inhomogeneous media," *Physical Review E*, vol. 71, no. 1, p. 016701, 2005.
- [31] J. Robinson *et al.*, "Electromagnetic simulations of microwave heating experiments using reaction vessels made out of silicon carbide," *Physical Chemistry Chemical Physics*, vol. 12, no. 36, pp. 10793-10800, 2010.
- [32] J. Robinson *et al.*, "Understanding microwave heating effects in single mode type cavities—theory and experiment," *Physical Chemistry Chemical Physics*, vol. 12, no. 18, pp. 4750-4758, 2010.
- [33] N. S. Bakhvalov and G. Panasenko, *Homogenisation: averaging processes in periodic media: mathematical problems in the mechanics of composite materials*. Springer Science & Business Media, 2012.
- [34] D. M. Pozar, *Microwave engineering*. John Wiley & Sons, 2009.
- [35] M. Kamiński, "Homogenization technique for transient heat transfer in unidirectional composites," *Communications in numerical methods in engineering*, vol. 19, no. 7, pp. 503-512, 2003.
- [36] B. Ashley, D. D. Lovingood, Y.-C. Chiu, H. Gao, J. Owens, and G. F. Strouse, "Specific effects in microwave chemistry explored through reactor vessel design, theory, and spectroscopy," *Physical Chemistry Chemical Physics*, vol. 17, no. 41, pp. 27317-27327, 2015.
- [37] S. Afandizadeh and E. A. Foumeny, "Design of packed bed reactors: guides to catalyst shape, size, and loading selection," *Applied thermal engineering*, vol. 21, no. 6, pp. 669-682, 2001.
- [38] W. Falter, C. H. Finkeldei, B. Jaeger, W. Keim, and K. A. N. Verkerk, "Isobutanol synthesis from syngas," in *Studies in surface science and catalysis*, vol. 119: Elsevier, 1998, pp. 465-471.
- [39] D. Geldart, "Types of gas fluidization," *Powder technology*, vol. 7, no. 5, pp. 285-292, 1973.
- [40] J. K. S. Wan and M. S. Ioffe, "Surface heating and energy transfer in pulsed microwave catalytic systems: A microwave-induced acoustic study," *Research on Chemical Intermediates*, vol. 20, no. 1, pp. 115-132, 1994.
- [41] G. S. J. Sturm, A. Q. V. B. Houckgeest, M. D. Verweij, T. Van Gerven, A. I. Stankiewicz, and G. D. Stefanidis, "Exploration of rectangular waveguides as a basis for microwave enhanced continuous flow chemistries," *Chemical Engineering Science*, vol. 89, pp. 196-205, 2013.
- [42] C. O. Kappe, "How to measure reaction temperature in microwave-heated transformations," *Chemical Society Reviews*, vol. 42, no. 12, pp. 4977-4990, 2013.
- [43] J. D. Moseley and C. O. Kappe, "A critical assessment of the greenness and energy efficiency of microwave-assisted organic synthesis," *Green Chemistry*, vol. 13, no. 4, pp. 794-806, 2011.

- [44] A. Holzwarth, J. Lou, T. A. Hatton, and P. E. Laibinis, "Enhanced microwave heating of nonpolar solvents by dispersed magnetic nanoparticles," *Industrial & engineering chemistry research*, vol. 37, no. 7, pp. 2701-2706, 1998.